Limiting angular momentum for statistical model description of fission

D. J. Hinde, A. C. Berriman, M. Dasgupta, J. R. Leigh, J. C. Mein, C. R. Morton, and J. O. Newton
Department of Nuclear Physics, Research School of Physical Sciences and Engineering, Australian National University, Canberra, ACT 0200, Australia

(Received 24 May 1999; published 27 September 1999)

Fission fragment cross sections and angular anisotropies have been measured to high accuracy for the $^{19}F+^{208}Pb$ reaction, together with evaporation residue cross sections, at bombarding energies from below the fusion barrier to 1.75 times the barrier energy. These data allow reliable calculations of the partial waves contributing to fission. Extensive statistical model calculations of the anisotropies are presented, including the effects of different fission transient delay times. The anisotropies at the highest bombarding energies can only be reproduced assuming that the fission barrier no longer controls the fission process when its height is less than the nuclear temperature. [S0556-2813(99)02910-6]

PACS number(s): 25.70.Jj

I. INTRODUCTION

The decay of compound nuclei by fission is usually described in terms of the statistical model, making use of the fact that the fission saddle-point configuration can be treated as a transition state [1] between the compound system in its quasiequilibrium condition, and the two separating fission fragments. In this picture, the level density at the transition state is critical in calculating fission properties. In particular, the dependence of the level density on excitation energy, mass asymmetry, and on projections of the total angular momentum, plays an important role in determining the prefission neutron multiplicity, the mass distribution and the fission fragment angular distribution respectively, as well as the overall fission probability.

In heavy-ion induced fission reactions, deviations of these measured quantities from the predictions of the statistical model have been used as evidence for the importance of dynamical aspects of fission, which are not included in the statistical model description. One of the most significant of these observables is the number of neutrons emitted before fission. The measurement of prefission (or more exactly prescission) neutron multiplicities in excess of statistical model predictions has been used to infer the characteristic dynamical time scale associated with the fission process. A number of analyses, such as Refs. [2–5], have concluded that the average minimum time for the evolution from the equilibrium deformation to the scission configuration is several 10^{-20} s.

Fission angular distributions have been perhaps even more widely studied, and are the main subject of this paper. Fission angular distributions are often characterized by the angular anisotropy A, defined as the ratio of the yield at $0°$ or $180°$ to that at $90°$, i.e., $A=W(180°)/W(90°)$. In heavy-ion induced fission reactions, the compound nuclei which undergo fission typically have high angular momentum. If fission of all nuclei occurred in the plane normal to the angular momentum, then the angular distribution would show a $1/\sin\theta$ behavior, where θ is the angle of observation with respect to the beam axis. However, because hot nuclei spontaneously change their shape (the fission process itself being a prime example), fragmentation can occur with the fission axis inclined away from the plane normal to the angular momentum vector. The probability of a given inclination is determined by a Boltzmann factor depending on the extra energy required to rotate the system with the axis perturbed from the normal. This can be expressed in terms of the projection of the total angular momentum onto the symmetry axis. It is useful to recall the expression for the rotational energy $E_{\rm rot}(J,K)$ of a nucleus with total angular momentum $J\hbar$ and projection $K\hbar$:

$$E_{\rm rot}(J,K)=\frac{\hbar^2(J^2-K^2)}{2\mathcal{J}_{\rm perp}}+\frac{\hbar^2K^2}{2\mathcal{J}_{\rm par}}, \tag{1}$$

where $\mathcal{J}_{\rm perp}$ and $\mathcal{J}_{\rm par}$ are respectively the moments of inertia perpendicular and parallel to the symmetry axis. The change in rotational energy associated with $K\neq 0$ is then

$$E_{\rm rot}(J,K)-E_{\rm rot}(J,0)=\frac{\hbar^2K^2}{2\mathcal{J}_{\rm par}}-\frac{\hbar^2K^2}{2\mathcal{J}_{\rm perp}}, \tag{2}$$

which reduces to

$$E_{\rm rot}(K)=\frac{\hbar^2K^2}{2\mathcal{J}_{\rm eff}} \tag{3}$$

when the effective moment of inertia $\mathcal{J}_{\rm eff}$ is defined as $(1/\mathcal{J}_{\rm eff})=(1/\mathcal{J}_{\rm par})-(1/\mathcal{J}_{\rm perp})$. It is usually assumed that $\mathcal{J}_{\rm eff}$ is independent of K; this assumption will be discussed in Sec. IV F.

It has been shown [6] that these expressions, together with the dependence of the saddle-point level density on $E_{\rm rot}(J,K)$, lead to a Gaussian distribution of K, centered around $K=0$, which is characterized by the variance K_0^2. This can be predicted within the statistical model, assuming compound nucleus formation, and a thermal distribution of the relevant variables. It is generally assumed that the projection M of the total angular momentum onto the space-fixed (beam) axis is zero. On this basis, fission angular distributions and thus anisotropies are calculated within the statistical model.

Fission fragment angular distributions have been measured extensively, particularly for heavy-ion reactions forming compound nuclei heavier than lead. For such reactions,

experimental values of A are often larger than those calculated. This has led to proposals that as well as fusion-fission, additional classes of fission exist.

Nonequilibrium fission [7] has been proposed as a distinctive fission process following a fusion reaction and subsequent compound nucleus formation inside the true fission saddle-point. It was postulated [7] that if the decay width is large, fission may take place after equilibration of all degrees of freedom except the K degree of freedom. A memory of the entrance channel K distribution should thus occur, and since the K value in the entrance channel is zero unless the projectile or target have intrinsic spin, nonequilibrium fission should usually have a large anisotropy.

Quasifission [8–10] is conceptually distinct from the proposed nonequilibrium fission process. Here, contact of the projectile and target nuclei is not followed by compound nucleus formation inside the fission saddle point. Instead, the shape of the nucleus, which is initially trapped inside the conditional saddle-point, evolves over the potential energy surface and the average trajectory passes outside the locus of conditional saddle points before reaching mass symmetry. Thus in principle there can always be some residual memory of the mass and direction of the projectile in the initial collision. Experimental data (for example, Ref. [10]) confirm this characteristic feature, particularly in association with projectiles heavier than ^{24}Mg. Measured values of A for quasi-fission reactions are larger than the statistical model predictions, which may be expected since the nuclei never become as compact as the equilibrium deformation, and also K equilibration is probably not attained.

Independent of experimental observations, it is expected that the statistical model picture will lose its validity for very high angular momenta, since ultimately the height of the fission barrier drops to zero. Under this condition, the concept of the saddle-point configuration as a transition point cannot be valid. Theoretical expectations and dynamical calculations [11] suggest that the fission saddle-point should already lose its effectiveness in controlling the fission process when the height of the fission barrier is reduced by angular momentum to a value similar to the nuclear temperature. Indeed, some time ago [12,13], measured anisotropies for heavy-ion induced fission were used to support this expected limit to the applicability of the statistical model picture.

Despite this, the statistical model is frequently used to describe reactions where, according to the above criteria, it should not be applicable. Depending on which criterion is used, the limiting angular momentum beyond which fission becomes purely a dynamical process can be quite different, particularly for heavy systems. To obtain experimental information on this limit, and to investigate how much other information on the fission process can be extracted from fission anisotropies, this paper describes a detailed comparison of data and calculated anisotropies. Particular emphasis is placed on the sensitivity of fission anisotropies to the parameters of the model, and recent advances in the understanding of the dynamics of both the fusion and fission processes are taken into account.

To achieve this aim, precise measurements were made of fission cross sections and angular anisotropies, and evaporation residue cross sections, for the ^{19}F+^{208}Pb reaction, forming the compound nucleus ^{227}Pa. Beam energies ranged from below to 1.75 times the mean barrier energy. This system was chosen for study because of the large anisotropies reported previously [14] at near- and sub-barrier energies. Analyses were carried out of both the sub-barrier anisotropies and of those at above-barrier energies. This paper concentrates on the above-barrier energies, while the sub-barrier results will be discussed in a separate paper, making use of the conclusions reached in the interpretation of the above-barrier data.

II. EXPERIMENTAL PROCEDURES

Measurements of fission fragments from the reaction ^{19}F+^{208}Pb were carried out using pulsed beams from the 14UD tandem electrostatic accelerator and LINAC at the Australian National University. The 14UD beam energy ranged from 82 to 135 MeV, with a pulse width of $\simeq 1$ ns, and a pulse separation of 106.6 ns. The four highest beam energies, up to 158 MeV, were obtained using the LINAC to boost the 14UD beam energy. The maximum beam energy spread introduced by the LINAC was 1.2 MeV, measured at the target position for the highest beam energy. The target of ^{208}PbS was $\simeq 25\,\mu$g cm^{-2} in thickness, evaporated onto a $\simeq 12\,\mu$g cm^{-2} C backing foil. The backing faced downstream, so as not to degrade the beam energy before interaction with the ^{208}Pb.

Fission fragments were detected in large area multiwire proportional counters (MWPCs), position sensitive in two dimensions. Each had an active width of 284 mm, and height 357 mm. The time signals from the position-sensing wires, separated by 1 mm, passed through delay lines with 1 ns delay between each wire, giving a position resolution of ≈ 1 mm. The detectors were placed 180 mm from the target, resulting in a scattering angle coverage of $-171° \leqslant \theta_{\rm lab} \leqslant -94°$ in the backward hemisphere, and $9° \leqslant \theta_{\rm lab} \leqslant 86°$ in the forward hemisphere. Signals in the forward detector were only accepted when in coincidence with the backward detector, to minimize dead time in the data acquisition system. The central foils of the MWPCs provided energy loss and timing signals. For each coincidence event, the positions (x,y) on the detectors were transformed to give the scattering angles $\theta_{\rm lab}$ with respect to the beam axis, and the azimuthal angles. This allowed the folding angle for the fission event to be determined. At all but the most backward angles, fission events following fusion of ^{19}F with ^{208}Pb were separated from other reaction products using the time of flight information from both back and front MWPC detectors, together with the folding angle information. The coincidence efficiency was less than unity because of the grid and window support wires of the front MWPC. The effect of these wires was measured at the higher beam energies where the fission yield was large, and fission events could be identified in the back angle MWPC alone without any ambiguity. Angle-averaged losses of 3% were found, in agreement with geometrical expectations. The data were corrected for losses

in each angle-bin individually. At angles backward of 155°, where the coincidence efficiency was diminished due to some of the coincident fission fragments being at too forward an angle to be detected in the front MWPC, the fission fragments were identified by the energy loss and time-of-flight information from the back MWPC alone. The kinematics of reactions on lighter nuclei present in the target meant that no contamination was present in the spectra at these angles.

The fission differential cross sections were obtained by calibrating each 5° wide bin in $\theta_{\rm lab}$ using Rutherford scattering at a sub-barrier energy with a ^{32}S beam on the ^{208}PbS target. Details of this procedure are described in Ref. [15]. Two Si surface-barrier detectors were positioned in the vertical plane, and were used to measure the elastically scattered yield, providing a normalization between the calibration and the fission excitation function measurements. At the lower beam energies, they were located at $\pm 22.5°$ relative to the beam axis, while for $E_{\rm lab} \geqslant 128$ MeV, they were positioned at $\pm 15.0°$, to ensure that the elastic differential cross-sections would follow the Rutherford scattering formula.

The evaporation residue (ER) cross sections were measured in a separate experiment by detecting the characteristic α particles emitted during the ground-state decay of the residues and their daughters. This was accomplished by stopping the ER in a catcher foil placed immediately behind the target, which in this measurement was ^{208}PbS of thickness $300\,\mu{\rm g\,cm^{-2}}$, on a $\simeq 15\,\mu{\rm g\,cm^{-2}}$ C backing. The catcher consisted of a sandwich of six Al foils, each of thickness $180\,\mu{\rm g\,cm^{-2}}$, giving a total thickness more than double the average range of the ERs at the highest beam energy used. An annular Si surface-barrier detector was located at a mean angle of 168.8° to detect the α particles. A pulsed beam of width 2.12 ms and period 10.60 ms was used, over a beam energy range of 83 to 103 MeV. Signals from the annular counter were recorded in a 7.96 ms interval during the beam-off period. Conveniently, essentially all ERs emit in their decay chain only one α-particle in the energy range 8.65 to 9.21 MeV, and with apparent lifetimes (due to parent decay lifetimes) between 6.2 ms and 2.6 s. For this reaction, no other source of α-particles within this energy range is expected. For the prevailing beam pulsing regime, the yield during the recording period was calculated to vary by less than 5% due to the different lifetimes within this range. Hence in view of the small fraction of fusion events leading to evaporation residues, the ER yields were determined from the total α-particle yield within this energy range, without identification of the individual decay channels. The solid angle of the annular counter relative to the sum of the solid angles of the two monitor detectors was determined by measuring in-beam elastic scattering at a sub-barrier energy, allowing the determination of the absolute ER cross sections.

III. EXPERIMENTAL ANALYSIS AND RESULTS

The aim of this work is to compare experimental and calculated fission anisotropies. It is not, however, sufficient to measure only the anisotropies. In order to make reliable calculations, the fusion cross sections and the fusion barrier distribution are required to calculate the compound nucleus angular momentum distributions, and the fission probability is required to determine the angular momentum distribution for the fission events alone. It is desirable to have prefission neutron multiplicity data to give experimental constraints on the mean temperature when passing the saddle point on the route to scission. The experimental data measured in this work to define these quantities are discussed below.

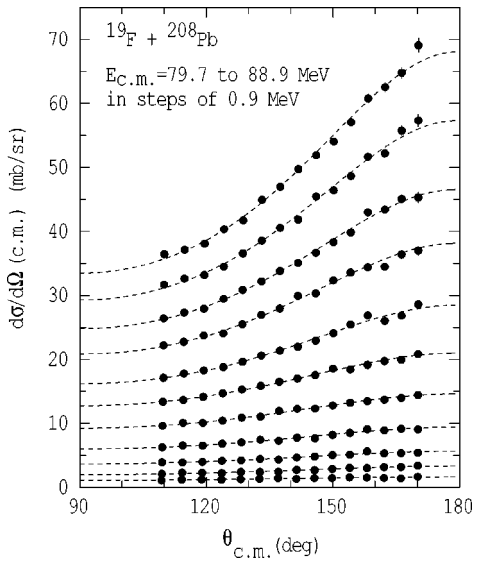

FIG. 1. Measured fission fragment angular distributions from $E_{\rm c.m.}=79.7$ to 88.9 MeV, after conversion to the center of mass frame. The transition state model fits are shown by the dashed lines, from which the fission anisotropies and cross-sections were determined.

A. Fission fragment angular distributions

The measured fission angular distribution must be converted from the laboratory to the center-of-mass frame. The fission folding angle distribution gives information on the kinematics of the reaction, and the distributions measured for this reaction were consistent, within experimental uncertainties, with fission following complete fusion at all beam energies. To avoid introducing additional random uncertainties into the data, the fission angular distributions were converted to the c.m. frame using the calculated velocity of the c.m. frame and mean fragment velocities evaluated from fission total kinetic energy systematics [16]. Typical measured angular distributions are shown in Fig. 1.

To determine the fission anisotropies and cross sections, it was necessary to extrapolate the measured angular distributions to both 180° and 90°. This was accomplished using the exact expressions of Back *et al.* [9], in an iterative procedure. Approximate fusion cross sections were used to generate the angular momentum distributions required to predict the shape of the fission angular distributions, from which fits to the data were obtained, and experimental fission cross sections determined. These were then used to determine more accurate angular momentum distributions, from which final fits were obtained, giving the anisotropies A and the fission cross sections $\sigma_{\rm fis}$, as well as the value of K_0^2, at each bombarding energy. In this analysis, it is implicitly assumed

that K_0^2 is independent of J. These fits are shown by the dashed lines in Fig. 1; they describe the data very well.

Since the analysis that follows relies on the accuracy and precision of the experimental results, sources of uncertainty in the measured quantities should be discussed. The experimental uncertainties in A result from three sources. Statistical uncertainties originate from the number of fission events detected. These uncertainties were small, at all but the lowest beam energies, due to the large solid angles of the MWPC detectors, which allowed typically 10^5 to 10^6 fissions to be collected in 30 min. Uncertainties also result from variation of the angle of entry of the beam into the target chamber, and the position of the beam spot on the target. These were calculated to result in a $\pm 2\%$ uncertainty in A. The third source of uncertainty is the extrapolation of the measured angular distribution to 180° and to 90°. As can be seen in Fig. 1, the wide angular acceptance of the fission detectors means that typically 85% of the total variation in differential cross-section between 90° and 180° is within the range of the data. Thus only 15% depends on the angular extrapolation. Since the fits describe the data very well, and are based on an exact theoretical calculation, we believe that the extrapolation does not contribute significantly to the experimental uncertainty for this reaction.

B. Evaporation residue and fission cross sections

Evaporation residue cross sections σ_{ER} were determined from the measured number of out-of-beam α particles detected, with normalization to the elastic scattering yield in two monitor detectors. Because the ER cross sections are low (less than 10 mb), experimental uncertainties originate predominantly from the relatively small number of α particles measured at each energy (at most a few thousand). The energy spectra themselves, being taken out-of-beam, were very clean. Systematic errors can be introduced through the use of a catcher foil which is too thin to stop all the ERs at the higher beam energies, however, due to the use of a thick catcher, this problem should not be present in these data.

The ER cross sections, shown in Fig. 2, display the typical saturation at high energies due to increasing fission competition. At the highest beam energy at which σ_{ER} was measured, the ER survival probability was barely over 1%.

Fission cross sections were determined from the fits to the angular distributions. Uncertainties in the cross sections have the same sources as for the anisotropies, however, since the cross sections are an integral quantity, the uncertainties are generally smaller. Simulations of the effect of possible beam axis and beam spot movement gave variations of less than 1% in cross sections. A repeat measurement was made during a different experiment, of a number of consecutive points at near-barrier energies, where it was suspected that one or two points were inconsistent with the general trends of the data. This revealed a satisfactory average deviation between the two measurements of only 1.4%, apart from one point which was 5% different. For all these energies, a weighted average of the two measurements was used. Both the fission and ER cross sections are shown in Fig. 2.

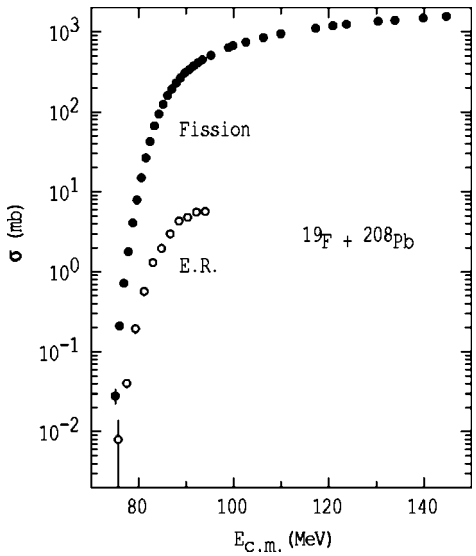

FIG. 2. Fission and evaporation residue (ER) cross sections measured in this work.

The best fit to all the fusion cross sections at above-barrier energies (see Sec. III C) was consistent with random uncertainties of $\pm 0.5\%$, and the fusion cross sections were assigned this uncertainty unless the statistical uncertainty due to the numbers of fission and ER events observed was larger, in which case the statistical uncertainty was used.

C. Fusion cross sections and barrier distribution

The fusion cross sections σ_{fus} were obtained by summing the measured fission and ER cross sections. At all energies, σ_{fis} was substantially greater than σ_{ER}, so the ER cross sections were interpolated to match the beam energies of the fission measurements. At the higher beam energies, where ER measurements were not made, σ_{ER} was assumed to remain at its saturation value of 5.8 mb, independent of beam energy. At the highest energy, this is less than 0.4% of the fusion yield, so a cross section of twice this value, or zero, would not significantly affect σ_{fus}. The resulting fusion excitation function is shown for the lower beam energies in Fig. 3(a).

The fusion barrier distribution [17], shown in Fig. 3(b), was determined from the second derivative with respect to the beam energy $E_{\mathrm{c.m.}}$, of the function $E_{\mathrm{c.m.}}\sigma_{\mathrm{fus}}$. A point-difference formula [18] was used, with an energy step of 1.83 MeV.

It has been shown [19,20] that for a given reaction, the fusion angular momentum distribution at any beam energy can be related to the fusion cross section and the fusion barrier distribution, through the fusion transmission coefficients. Experimental confirmation of this expectation has come from fusion reactions for which fission is not a significant decay mode. Here, barrier distribution models which reproduce the measured fusion excitation function generally reproduce the experimental mean angular momentum $\langle L \rangle$ determined by a variety of techniques. These include isomer ratio measurements, mean γ-ray multiplicities, feeding patterns to the

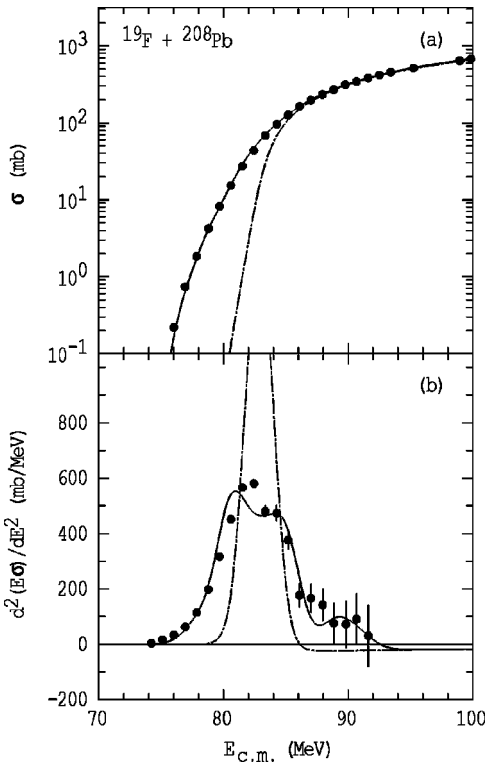

FIG. 3. The measured fusion excitation function (a) and experimental fusion barrier distribution (b), shown for the lower beam energies. A single barrier (no coupling) fusion calculation fitted to the high energy fusion cross sections is shown in (a), together with the corresponding barrier distribution in (b), by the dot-dashed lines. The results of a coupled-channels calculation which gave a good fit to the data at all energies is shown by the full lines (see text).

ground-state rotational band, and ratios of xn evaporation residue yields [21].

By fitting the measured fusion cross sections with a realistic model, and ensuring that the shape of the barrier distribution is reproduced, reliable predictions of the angular momentum distributions should be obtained. The fusion angular momentum distributions for this reaction were determined by first fitting the above-barrier cross sections using a version of the simplified coupled-channels code CCMOD [22,23], derived from the code CCFUS [24]. A Woods-Saxon nuclear potential of fixed depth 50 MeV was used, and the radius parameter and diffuseness parameter were varied, the best-fitting values being 1.168 and 1.01 fm, respectively. Then couplings to states in ^{208}Pb and ^{19}F were included, making use of the couplings required in other reactions [25], which resulted in a good fit to the whole excitation function. In this work, it is only the fit to the data which is needed to predict the angular momentum distributions, so details of the couplings used are not discussed here, but will be in a forthcoming paper. The calculation which best reproduced the cross sections and barrier distribution is shown in Figs. 3(a) and 3(b) by the full lines. A tabulation of the experimental fusion and ER cross sections, and the fission anisotropies and their uncertainties is given in Table I.

IV. TRANSITION STATE MODEL CALCULATIONS

The fission angular anisotropies were calculated within the transition-state–statistical-model picture as described in Ref. [15], using the exact expressions of Ref. [9]. The combination of precisely measured anisotropies, and a detailed measurement of the dependence on beam energy is still not so common. For this reason, an in-depth comparison of the data with calculations was considered worthwhile.

Fission anisotropies are affected by many physical effects during the fission process, and by the values of critical parameters in statistical model calculations. Some of these simply scale the calculated anisotropies in an energy-independent way, such that a change in one parameter can be offset by a change in another. Others have a weak dependence on beam energy, while a few can change the beam energy dependence substantially.

In the following description of the comparison of data and calculations, some effects which are discussed have not been explicitly included in the calculations, when they are judged to be in the first or second of the above categories, and their effect on the anisotropies is calculated or estimated to be less than 5%. The dependence of the calculated anisotropy on the input parameters can be most easily seen from the approximate expression for the anisotropy

$$A = W(180°)/W(90°) \approx 1 + \frac{\langle J^2 \rangle}{4K_0^2} = 1 + \frac{\langle J^2 \rangle \hbar^2}{4T\mathcal{J}_{\rm eff}}, \qquad (4)$$

where $\mathcal{J}_{\rm eff}$ and the temperature T refer to the saddle point. $J\hbar$ is the angular momentum at the saddle point, which is closely related to the orbital angular momentum $L\hbar$ brought in by the projectile, the small change in angular momentum being due to presaddle particle evaporation. The evaporation process was modelled using the Monte Carlo statistical model code JOANNE2 [5]. The ground-state spin of the projectile is small ($\frac{1}{2}$) compared with typical values of K_0, and its effect has been neglected. It was pointed out in Ref. [12] that perturbation of the initial M substate distribution (taken here as $M=0$) by presaddle evaporation may in some cases significantly affect the calculated anisotropies. For the ^{19}F+^{208}Pb reaction the presaddle multiplicity is typically one third of that in Ref. [12], and thus the effect on the ^{19}F+^{208}Pb anisotropies is estimated to be typically less than 5%. The rather weak beam energy dependence of the presaddle multiplicity, as can be seen from the dashed or dot-dashed lines in Fig. 6(a), implies a similarly weak dependence of the correction on beam energy. For these reasons, in this work no correction was applied to the calculated A values.

The effective moment of inertia, as a function of angular momentum, was taken from the rotating finite range model (RFRM) calculations [26]. The change in $\mathcal{J}_{\rm eff}$ after evaporation of one or two neutrons is negligible, so the calculated values for ^{227}Pa were used for all nuclei in the decay chain. The small difference between $\mathcal{J}_{\rm eff}$ for ^{227}Pa and ^{225}Pa is illustrated in Fig. 7(a). For $J>72$, where the fission barrier height is calculated to be zero, the value of $\mathcal{J}_{\rm eff}$ for $J=72$ was used initially in the calculations.

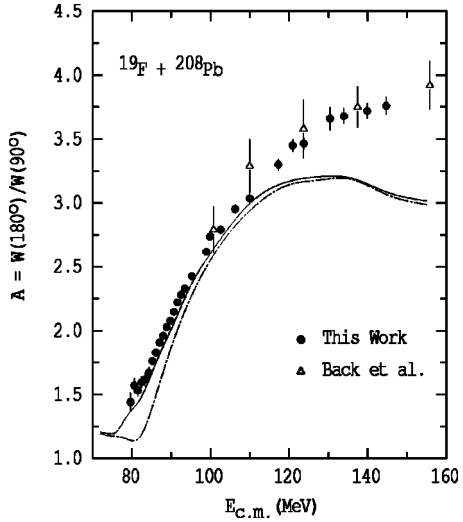

FIG. 4. Fission anisotropies for the fusion of ^{19}F with ^{208}Pb, measured in this work (full circles) and taken from Ref. [9] (triangles). The full line represents the A values resulting from statistical model calculations for ''standard'' parameters (see text), using angular momentum distributions from the best-fitting coupled-channels fusion calculation (see Fig. 3). The dot-dashed line shows the A values using the fusion angular momentum distributions resulting from the single fusion barrier calculation.

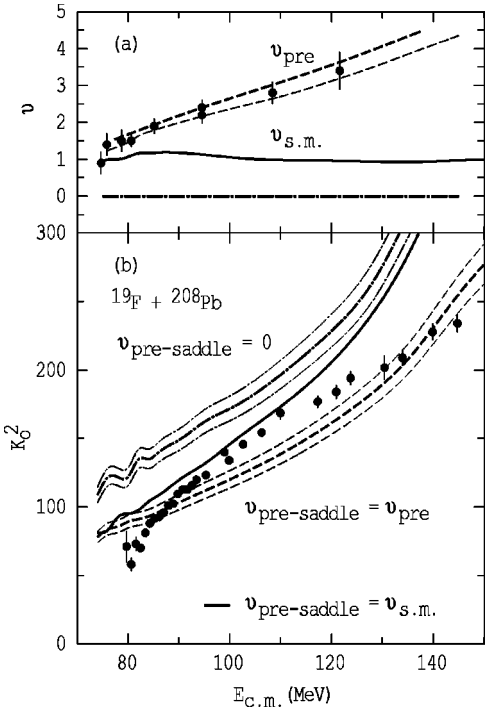

FIG. 5. (a) The measured prescission neutron multiplicities for the reaction ^{16}O+^{208}Pb (circles). Multiplicities calculated with the statistical model are shown, using parameters adjusted to give $\nu_{\text{presaddle}}=0$ (thick dot-dashed line), and to give the maximum values allowed by the data $\nu_{\text{presaddle}}=\nu_{\text{pre}}$ (thick dashed line). For the latter case, a calculation using the same statistical model parameters, but for ^{19}F+^{208}Pb, is indicated by the thin dashed line. The full line labeled $\nu_{\text{s.m.}}$ is a calculation for ^{19}F+^{208}Pb using the ''standard'' statistical model parameters (see text). (b) The corresponding calculated values of K_0^2 are shown as a function of beam energy for the ^{19}F+^{208}Pb reaction, compared with the values of K_0^2 extracted from the measured anisotropies for that reaction. The thin dashed and dot-dashed lines indicate the effects of varying the saddle-point level density parameter by $\pm 10\%$.

The temperature at the saddle point will actually have a distribution, due to the variation in the number and kinetic energy of neutrons emitted before passing over the saddle point. This distribution depends on J, as does $\mathcal{J}_{\text{eff}}$. The code JOANNE2 allows these correlations to be taken into account by calculating the number of fission events at each element in a matrix of T and J. Then, using the appropriate $\mathcal{J}_{\text{eff}}$ for each J, the value of K_0^2 is calculated for each element, including the postscission reorientation term [9]. By weighting these values by the number of events in each bin of T and J, the calculated average K_0^2 and A then correspond closely to the actual situation, within the framework of the transition state model.

A. Defining standard statistical model parameters

In making statistical model calculations, values have to be assigned to the parameters describing the decay process. The T distribution is related to the presaddle neutron multiplicity ($\nu_{\text{presaddle}}$). It has been shown [27] that in statistical model calculations for this mass region, $\nu_{\text{presaddle}}$ is most sensitive to the ratio of the level density parameter at the saddle-point configuration (a_f) to that at the equilibrium deformation (a_n). According to theoretical calculations [28], a_f/a_n is predicted to be 1.05 for ^{227}Pa, at $J=0$. However, to reproduce the measured prefission neutron multiplicities ν_{pre} for similar systems [29] measured at low excitation energies, where the effects of the dynamical fission timescale should be small, values of a_f/a_n between 0.98 and 1.02 were needed. The value 1.02 was chosen for the calculations, with a_f set to $A/8.8$ [28].

A Kramers' scaling factor, which suppressed the fission width by 2.5, allowed the measured fission probabilities to be matched at a number of beam energies spanning the data. The fission probability could equally well have been reproduced by scaling the fission barrier height. However, since $\mathcal{J}_{\text{eff}}$ and the calculated fission barrier height are related in the RFRM calculations, in principle, scaling of the fission barrier should be accompanied by a change in the $\mathcal{J}_{\text{eff}}$.

The initial compound nucleus is formed at excitation energies between 30 and 95 MeV, however, this paper concentrates on the higher energies, so the mass excesses of all product nuclei were taken from the liquid drop model, without shell or pairing corrections. $\mathcal{J}_{\text{eff}}$ was also taken to be unaffected by any shell corrections at the saddle point. The compound nucleus ^{227}Pa is far from a spherical closed shell, and ground-state shell corrections are small.

B. Sensitivity to fusion L distributions

Calculations were performed to check the sensitivity of the calculated A values to the fusion L distributions. Initially the L distributions obtained from the best fit to the fusion data, as described in Sec. III C, were used. The calculated A

values are shown in Fig. 4 by the full line. Then anisotropies were calculated for L distributions resulting from a fusion calculation without any coupling included. This resulted in calculated A values indicated by the dot-dashed line in Fig. 4. At energies near and below the fusion barrier, the results of the two calculations are very different. At higher energies, there is only a small decrease in the anisotropy when the couplings are neglected, as would be expected, and thus in this energy region, uncertainty in the angular momentum distribution should make a negligible contribution to the uncertainty in the calculations.

C. Presaddle neutron emission

The observed strong increase of A with beam energy is due to the increase in the fusion cross section, whose product with $E_{\mathrm{c.m.}}$ is directly proportional to the mean value of L^2. Since the L distributions are believed to be well-known because of the good fit to the precise fusion data, it should be appropriate to present the data in terms of the values of $K_0^2 = (T\mathcal{J}_{\mathrm{eff}})/\hbar^2$ deduced from the fits to the measured angular distributions as described in Sec. III A. Although presentation of data and calculations in terms of the anisotropies could be preferable, since the deduced A values are independent of the fusion model used, small changes in the saddle point conditions tend to be masked by the larger changes in $\langle J^2 \rangle$ with $E_{\mathrm{c.m.}}$. Since K_0^2 is determined by saddle-point properties alone, presentation in terms of the deduced K_0^2 shows changes in these properties with $E_{\mathrm{c.m.}}$ more clearly. Data for other reactions have commonly been presented in this way. However, it will be demonstrated later that comparison of calculations and data in terms of K_0^2 can be slightly misleading, particularly where a wide range of J is present.

Initial comparisons of data and calculations are made in terms of K_0^2, the deduced experimental values being shown in Fig. 5(b) as a function of $E_{\mathrm{c.m.}}$. They show a smooth and consistent increase with increasing beam energy. The values and energy dependence of K_0^2 may be expected to be determined mainly by the variation of the saddle-point temperatures with beam energy, since the values of $\mathcal{J}_{\mathrm{eff}}$, as calculated with the RFRM, do not change appreciably with angular momentum until close to the angular momentum where the fission barrier height falls to zero. The saddle-point temperature depends on the level density parameter at the saddle-point a_f, and on the excitation energy above the saddle point. The mean excitation energy could be determined if the number of neutrons emitted before crossing the saddle point ($\nu_{\mathrm{presaddle}}$) was known. However, experimentally it appears to be impossible to characterize neutrons as being emitted presaddle or postsaddle.

Theoretically, if neutron emission lifetimes are much longer than the time to pass from the saddle point to the scission configuration (which may be $\sim 10^{-20}$ s), the measured prescission neutron multiplicity ν_{pre} can be identified with $\nu_{\mathrm{presaddle}}$. If the lifetimes are similar or shorter, then part of ν_{pre} will result from postsaddle emission, and in this case, $\nu_{\mathrm{presaddle}}$ will be less than ν_{pre}. Thus at low excitation energies (E_x), where the statistical model lifetime is long compared to dynamical fission time scales, $\nu_{\mathrm{presaddle}}$ may be identified with the measured ν_{pre}.

TABLE I. The fusion cross sections, ER cross sections, and fission anisotropies at the center-of-mass energies $E_{\mathrm{c.m.}}$. For the ER data, 0.32 MeV should be subtracted from $E_{\mathrm{c.m.}}$ to account for the target being thicker than that used for the fission measurement (see text).

$E_{\mathrm{c.m.}}$ (MeV)	σ (mb)	$\delta\sigma$ (mb)	σ_{ER} (mb)	$\delta\sigma_{\mathrm{ER}}$ (mb)	A	δA
76.0	0.22	0.02	0.008	0.006		
76.9	0.74	0.03				
77.9	1.83	0.04	0.04	0.005		
78.8	4.22	0.06				
79.7	8.17	0.09	0.195	0.026	1.44	0.08
80.6	15.4	0.1			1.57	0.06
81.5	27.3	0.2	0.57	0.04	1.53	0.05
82.4	43.6	0.2			1.60	0.04
83.4	68.2	0.3	1.31	0.10	1.62	0.05
84.3	95.7	0.5			1.67	0.04
85.2	126	0.6	1.96	0.12	1.76	0.02
86.1	163	0.8			1.83	0.02
87.0	197	1	2.99	0.18	1.91	0.02
87.9	234	1			1.96	0.02
88.9	271	1	4.32	0.23	2.03	0.02
89.8	313	2			2.08	0.02
90.7	344	2	4.81	0.3	2.15	0.02
91.6	382	2			2.22	0.02
92.5	418	2	5.58	0.3	2.28	0.01
93.4	454	2			2.33	0.02
95.3	515	3	5.69[a]	0.3	2.43	0.02
99.0	643	3			2.62	0.02
99.9	679	3			2.74	0.03
102.6	749	4			2.79	0.02
106.3	856	4			2.95	0.04
109.9	953	5			3.04	0.05
117.3	1116	6			3.30	0.05
120.9	1200	6			3.45	0.05
123.7	1250	6			3.47	0.05
130.4	1364	7			3.66	0.09
133.9	1403	7			3.68	0.06
139.9	1493	7			3.72	0.06
144.7	1567	8			3.76	0.07

[a]Actual measurement made at $E_{\mathrm{c.m.}} = 94.0$ MeV.

The number of neutrons emitted before scission has been measured over a range of energies for fission following the fusion of ^{16}O with ^{208}Pb [2,30], forming the compound nucleus ^{224}Th, a neighboring compound nucleus to ^{227}Pa. Since calculated multiplicities are similar for the two reactions, (see below) comparisons of calculations for ^{19}F+^{208}Pb with the ν_{pre} data for ^{16}O+^{208}Pb is both reasonable, and useful.

D. Calculations for two extremes of T

Initially, statistical model calculations were performed for two extreme scenarios, namely, where $\nu_{\mathrm{presaddle}} = \nu_{\mathrm{pre}}$, or

where $\nu_{\text{presaddle}}=0$, corresponding to the lowest and highest possible mean saddle-point temperatures, respectively. In these and the following calculations, the angular momentum distributions calculated from the best fit to the fusion data were used.

Two statistical model parameter sets were chosen, which either gave the maximum neutron multiplicities consistent with the measured ν_{pre} values for the $^{16}O+^{208}Pb$ reaction, or which resulted in essentially no presaddle neutrons. The former calculation required $a_f/a_n=0.91$, whilst for the latter, $a_f/a_n=1.2$ was used. The level density parameters were adjusted so that a_f still retained the value $A/8.8$ for these calculations, thus the variation in the calculated T was only due to the change in excitation energy at the saddlepoint. The fact that the measured ν_{pre} values can be reproduced with the statistical model for this reaction should not be taken to mean that the value of $a_f/a_n=0.91$ is correct, nor that there is no need to invoke dynamical effects. For lighter, less fissile compound nuclei (for example, ^{213}Fr, ^{200}Pb [29]) the minimum value of a_f/a_n required to fit the low excitation energy ν_{pre} data is 0.98 ± 0.02 without the inclusion of any dynamical effects [29], while $a_f/a_n=1.02\pm0.02$ reproduces experimental data well when the dynamical time scale required to fit the higher energy data is included [29,31].

The calculated neutron multiplicities corresponding to $\nu_{\text{presaddle}}=\nu_{\text{pre}}$ are shown in Fig. 5(a) for the $^{16}O+^{208}Pb$ reaction by the thick dashed line, together with the experimental data, and for the $^{19}F+^{208}Pb$ reaction, using the same statistical model parameters, by the thin dashed line. The thick dot-dashed line indicates the $\nu_{\text{presaddle}}=0$ calculation. The calculated K_0^2 values for the $^{19}F+^{208}Pb$ reaction corresponding to these two extreme scenarios are indicated in Fig. 5(b) by the thick dashed line ($\nu_{\text{presaddle}}=\nu_{\text{pre}}$) and the thick dot-dashed line ($\nu_{\text{presaddle}}=0$). The experimental K_0^2 data on average lie closest to the $\nu_{\text{presaddle}}=\nu_{\text{pre}}$ line, but the form of the energy dependence is different from the calculation. The actual temperature distribution at the saddle-point would be expected to lie at some point between these limits, however, as will be seen in Fig. 6, this point is likely to be energy dependent.

To show the sensitivity of the calculations to a_f, the effect of a $\pm10\%$ change from the assigned value of $a_f=A/8.8$ (while retaining the values of a_f/a_n assigned) is indicated by the fine dashed and dot-dashed lines. As expected, this simply results in a change in the calculated K_0^2 values by $\pm5\%$, which is a small effect compared to the difference between the two neutron emission scenarios. The results of the calculation performed with the ''standard'' statistical model parameters, as described in Sec. IV A, is given by the full lines in Figs. 5(a) and 5(b). This describes rather better the experimental energy dependence of K_0^2 up to 110 MeV, except for the very lowest energies, where the data lie below all the calculations. This disagreement at low energies could possibly be associated with the fusion angular momentum distributions at the sub-barrier energies, the ER survival probability, and/or the calculations of the temperature distributions at low E_x. These questions will be discussed in a separate paper. This local disagreement should not affect comparisons of calculations and data at higher energies, since the proposed explanations only significantly affect the results at the lowest beam energies.

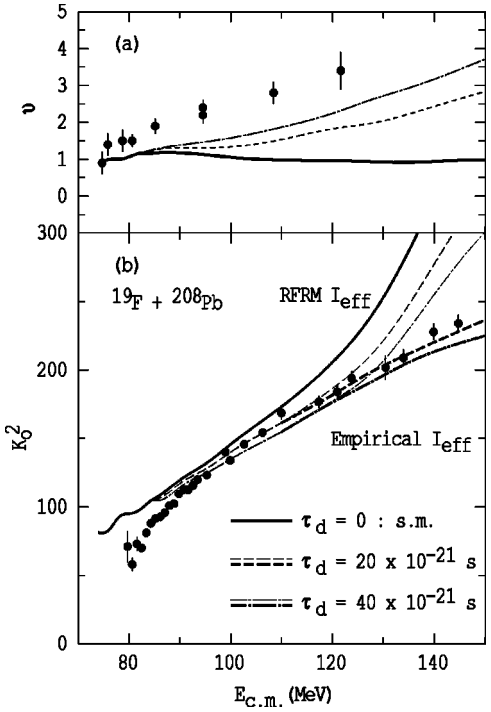

FIG. 6. Same as Fig. 5, except that the calculations are all for $^{19}F+^{208}Pb$, the full line being the ''standard'' statistical model calculations, and the dashed and dot-dashed lines showing the effect of transient delay times of 20×10^{-21} s and 40×10^{-21} s, respectively. The thick dashed and dot-dashed lines in the lower panel show that the K_0^2 data above 90 MeV can be reproduced satisfactorily using the two ''empirical'' angular momentum dependent effective moment of inertia curves [see Fig. 7(a)].

E. Inclusion of fission transient delay

The values of $\nu_{\text{presaddle}}$ from the ''standard'' calculation lie far below the measured ν_{pre} at the higher energies. This discrepancy is well known, and has been attributed to both neutron emission during the transient delay time between thermal equilibrium and the attainment of the quasistationary fission width (flux) over the saddle-point, and neutron emission during the transition from the saddle-point to scission. The transient delay may be thought of as the time to reach full shape equilibration in the potential pocket. This effect can be modelled in the simplest way [2] by introducing into the statistical model calculations a fixed delay time (τ_d), during which evaporation is allowed, but fission is forbidden.

Calculations were performed for τ_d values of 20×10^{-21} s and 40×10^{-21} s. The resulting neutron multiplicities and K_0^2 values are shown in Fig. 6(a) and 6(b) by the fine dashed and dot-dashed lines, and are compared with the ''standard'' statistical model calculations, shown by the full lines. As expected, at low E_x where the statistical model lifetime is long, the effect of the transient delay is negligible, and as E_x increases, the effect becomes larger. The resulting decrease in T at the saddle-point leads to a better agreement

between the calculated and measured K_0^2, as shown previously [32]. Delay times longer than 40×10^{-21} s give temperatures too low (and thus K_0^2 too low), best agreement apparently occurring for $\tau_d=20\times10^{-21}$ s, at least up to $E_{\text{c.m.}}=120$ MeV. Beyond this point, the calculated K_0^2 values rise rapidly, and even the assumption that all neutrons are emitted presaddle fails to reproduce the data at the highest energies [see Fig. 5(b)], while substantially under-predicting the K_0^2 data between $E_{\text{c.m.}}=90$ MeV and 120 MeV. The fact that ν_{pre} is under-predicted by the transient delay times assigned is consistent with substantial neutron emission after passing the saddle point, which may be inferred from other experimental evidence [4].

F. Modification of RFRM $\mathcal{J}_{\text{eff}}$

The reason for the rapid rise in the calculated K_0^2 values at the higher beam energies can be found by inspecting the RFRM calculated dependence of $\mathcal{J}_{\text{eff}}$ on angular momentum J, shown in Fig. 7(a) for ^{227}Pa by the thick full line. The rapid rise at high angular momentum is due to the ''shrinking back'' of the saddle-point deformation to meet the equilibrium deformation at the angular momentum where the fission barrier height falls to zero [see Fig. 7(b)]. This is calculated to occur at $J=73$ for ^{227}Pa.

The values of K_0^2 deduced from the measurement are not consistent with this rise in $\mathcal{J}_{\text{eff}}$, within the framework of the statistical model, even when modified to include the effect of a transient delay. The simplest way to obtain agreement with the data (following Back [33]) is to change the dependence of $\mathcal{J}_{\text{eff}}$ on J. To obtain an energy dependence to match the data, an ''empirical'' $\mathcal{J}_{\text{eff}}$ was generated, beginning to deviate from the RFRM calculations at a certain J value, and with a simple linear dependence on J. The energy dependence of the data could be reproduced assuming the ''empirical'' $\mathcal{J}_{\text{eff}}$ shown by the dashed line in Fig. 7(a), for a delay time of 20×10^{-21} s, and by the dot-dashed line for 40×10^{-21} s. These resulted in the calculated K_0^2 values as indicated in Fig. 6(b) by the thick dotted and dot-dashed lines, respectively. A slight change in the level density parameter (and thus saddle-point temperatures) for one of the calculations would bring both into very close agreement, and the overall agreement with the trends of the data is excellent. The deviation from the RFRM calculation occurs at $J=50$ and $J=60$ for $\tau_d=20\times10^{-21}$ s and 40×10^{-21} s, respectively.

It must be pointed out that the K_0^2 data between 90 and 120 MeV can be reproduced by various combinations of scaling the RFRM $\mathcal{J}_{\text{eff}}$, and varying a_f and τ_d. As long as these data are reproduced, the calculations using the RFRM $\mathcal{J}_{\text{eff}}$ will still deviate from the data at around 120 MeV. Thus the angular momentum at which the ''empirical'' $\mathcal{J}_{\text{eff}}$ deviates from the RFRM calculations will not be significantly different.

The calculated partial wave distributions for various beam energies are shown in Fig. 7(c), together with the RFRM calculated equilibrium and saddle-point rotational energies, plotted with respect to the LDM ground state. This figure, when compared with Fig. 7(b), shows clearly how the fraction of events with low fission barrier heights becomes significant as the beam energy increases. Comparison with Fig. 7(a) shows at what energies the ''empirical'' $\mathcal{J}_{\text{eff}}$ comes into play. The partial wave distributions show structure at the highest angular momentum which reflects the structure in the calculated fusion barrier distribution [see Fig. 3(b)].

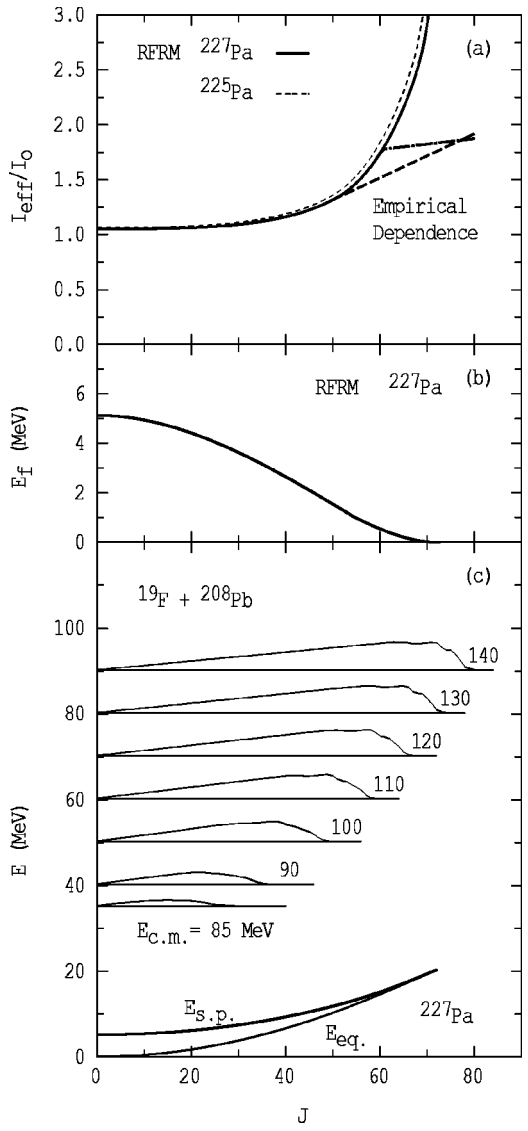

FIG. 7. (a) The ratio of the effective moment of inertia ($\mathcal{J}_{\text{eff}}$) to that of the equivalent sharp-surfaced sphere ($\mathcal{J}_0$), as a function of angular momentum $J\hbar$, for ^{227}Pa (thick lines) and ^{225}Pa (thin dashed line). The ''empirical'' dependence required to reproduce the trends of the K_0^2 data [see Fig. 6(b)] are indicated by the dashed and dot-dashed lines. (b) RFRM calculated fission barrier height as a function of J for ^{227}Pa. (c) RFRM calculated energy of the rotating equilibrium deformation (E_{eq}) and of the rotating saddle-point ($E_{\text{s.p.}}$) as a function of J. The calculated fusion L distributions from the best fit to the fusion data (see Fig. 3) are shown for various beam energies, at their excitation energies above the LDM ground state.

A comparison of data and calculations in terms of the measured anisotropies is made in Fig. 8, where again it can

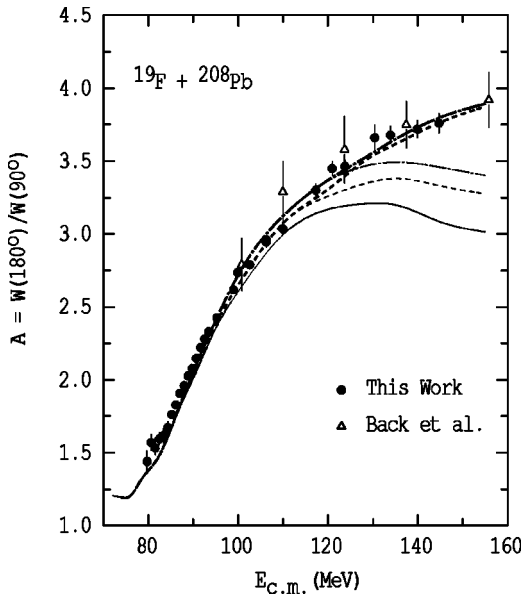

FIG. 8. Comparison of measured fission anisotropies with modified statistical model calculations, as a function of beam energy. Lines with the same style as those in Fig. 6(b) correspond to the same calculation. The data at all but the lowest energies are very well reproduced by including both a transient fission delay and a modified $\mathcal{J}_{\rm eff}$ as shown in Fig. 7(a).

be seen that the model calculations with RFRM $\mathcal{J}_{\rm eff}$ values (thin lines) do not have the correct energy dependence, while with the modified $\mathcal{J}_{\rm eff}$ (thick lines), the agreement is, as expected, excellent. In comparing these calculations with the anisotropy and the deduced K_0^2 values, it is apparent that the calculation giving best agreement with K_0^2 does not give the best agreement with A at the highest energies. This discrepancy can be traced to the assumption in the extraction of K_0^2 from the measured A values, that a single value of K_0^2 applies, independent of angular momentum. In reality, and in the calculations of A, K_0^2 is correlated with J, so the ultimate comparison of data and calculations should be carried out with the anisotropies, or even more correctly, with the fission angular distributions themselves.

It is appropriate here to discuss the commonly made assumption that $\mathcal{J}_{\rm eff}$ is independent of K. Calculations for the reaction measured in this work were made in Ref. [34] with the flexible rotor model, which includes the response of the nuclear shape to $K\neq 0$. It was shown that at $E_{\rm c.m.}=124$ MeV, the anisotropy is increased by just 0.1. If the size of the effect is proportional to K_0^2, an increase by 0.05 at 90 MeV might be expected. For this reaction, at the energies studied, it appears that the assumption that $\mathcal{J}_{\rm eff}$ is independent of K is quite reasonable. It is likely that other uncertainties in the calculations are at least as large, however, in principle this effect should not be neglected when comparing calculations and data.

The implications of the modifications to the standard statistical model required to reproduce the measured energy dependence of these data are discussed in the next section.

V. DISCUSSION

The experimental data have been reproduced through two modifications to the standard statistical model. The first is the introduction of a transient delay time, which is well established through both theoretical predictions [35], and the evidence of a large body of $\nu_{\rm pre}$ data, for example, Refs. [2–4, 29, 36–42], which exceed the predictions of statistical model calculations, thus requiring a dynamical timescale for fission which is long compared to the lifetime for particle evaporation.

It is necessary to discuss briefly the correlation between the level density parameters and the delay times needed to fit the data, before returning to the main argument of the paper. The delay time required to fit the present anisotropy data depends sensitively on the level density parameters chosen, since the neutron emission width and thus the number of neutrons emitted during the transient delay depends on a_n, while the temperature at the saddle-point (and thus K_0^2) depends on a_f. With $a_n=A/8.63$ and $a_f=A/8.8$ ($a_f/a_n=1.02$) a delay time between 20 and 40×10^{-21} s was required to reproduce the K_0^2 data between 90 and 120 MeV. Changing a_f/a_n to 1.05, as calculated for $J=0$ using the formula of Ref. [28], does not significantly change $\nu_{\rm presaddle}$ at the higher energies, since the statistical model values of $\nu_{\rm presaddle}$ are already small for $a_f/a_n=1.02$, and the effect of increasing a_f/a_n will be partly compensated by an increase in the number of neutrons emitted during the transient delay. If $a_f=A/8.0$ were chosen (retaining $a_f/a_n=1.02$), only a very short delay time would be required to fit the K_0^2 data up to 120 MeV. With this delay time, $\nu_{\rm presaddle}$ would, however, be small, and most of the observed neutrons would have to be emitted postsaddle. Conversely, a value of $a_f=A/9.7$ would require a longer delay time to reproduce the K_0^2 data, and give a small postsaddle multiplicity. It is not possible to tightly constrain the values of a_f, a_n, and τ_d with the data presented, although a reasonably good reproduction of the data can be obtained with the ''standard'' parameters, and the value of τ_d required is consistent with that deduced from other data. Further studies of complete data sets, including fission probabilities, prefission neutron data, and also, ideally, particle emission energy spectra in coincidence both with fission and evaporation residues, should ultimately allow the complex multichance, dynamically affected fission process following heavy-ion fusion reactions to be fully understood. Fission anisotropies should play a vital role, being sensitive to the temperature distribution at the saddle-point.

Returning to the main argument of the paper, it was concluded that no reasonable changes in the model parameters were able to reproduce the K_0^2 data at the highest energies, where the RFRM predicts a rapid increase in $\mathcal{J}_{\rm eff}$ at high J, causing the calculated anisotropies to fall, while the measured values continue to rise.

Modification of the RFRM $\mathcal{J}_{\rm eff}$ values at high J allowed agreement between the data and calculations to be achieved. In the current analysis of the new data for the ^{19}F+^{208}Pb reaction, it was found that the data prohibited a decrease in $\mathcal{J}_{\rm eff}$, as proposed in Ref. [33], but rather required that $\mathcal{J}_{\rm eff}$ should not increase as rapidly as the RFRM predicts. The

angular momentum at which the ''empirical'' $\mathcal{J}_{\rm eff}$ deviates from the calculated values appears to lie between $J=50$ and $J=60$. This corresponds to $T=0$ fission barrier heights between approximately 1.5 and 0.5 MeV.

Our interpretation of this observation is neither that there must be a unique nuclear shape which controls the fission anisotropy, corresponding to the ''empirical'' $\mathcal{J}_{\rm eff}$ value, nor that the entire reaction process changes its character dramatically once the RFRM value of $\mathcal{J}_{\rm eff}$ apparently become inappropriate—we do not suggest that the reaction becomes suddenly a quasifission process. The fact that the deviation from the statistical model picture starts to occur at angular momenta where the fission barrier height is less than the saddle-point temperature ($T\sim 1.6$ MeV) suggests strongly that the reason for the failure of the statistical model picture is that it is no longer valid if the fission barrier could be passed at the first attempt. Then, all the properties of the fission process should be determined completely by the dynamics of the motion over the potential energy surface.

Under these circumstances, why should the fission K distribution be narrower (i.e., have a smaller K_0^2) than predicted by the statistical model?

The distribution of K values at the saddle-point can be thought of as arising in the following manner. If the system is trapped in the potential pocket corresponding to the compact equilibrium deformation, the generation of shapes with $K\neq 0$ can be attributed to the Brownian motion of the shape coordinates, resulting in a wide distribution of angles between the longest axis and the direction of the angular momentum vector, due to the very large $\mathcal{J}_{\rm eff}$ associated with the compact equilibrium shape [see Eq. (3)]. In the statistical model, the saddle point acts as a filter of this wide K distribution, selecting those configurations with K closer to zero. This filtering results from the greater reduction in level density at the saddle point when K deviates from zero, due to the saddle-point shape being necessarily more elongated than the equilibrium shape, and thus having a smaller $\mathcal{J}_{\rm eff}$.

In a fully dynamical model, the trajectories over the multidimensional potential energy surface in principle determine all the properties of the fission process. Assuming that all trajectories passed through the equilibrium pocket, it would be envisaged that a distribution of K wider than that at the saddle point would result, for the following reason. The energy required to generate $K=20$, for $J=60$ at the equilibrium deformation, is estimated to be only 0.3 MeV, compared with 1.2 MeV at the saddle point. The time required to generate a distribution of K through shape fluctuations costing only 0.3 MeV of deformation energy would seem unlikely to be more than the time required to overcome a fission barrier of height ~ 1 MeV.

If in contrast it were assumed that not all trajectories necessarily pass through the equilibrium deformation, a K distribution narrower than that at the saddle point could result. It would be expected that at low J, where the fission barrier height is ~ 5 MeV, all, or almost all the trajectories would indeed pass through the equilibrium deformation. At higher J, where the fission barrier height is less then the temperature, a significant fraction of trajectories may never reach the compact equilibrium shape. The K distribution for these trajectories could be narrower, because some of the trajectories may never reach a shape as compact as the saddle-point shape calculated with the RFRM. Thus the maximal $\mathcal{J}_{\rm eff}$ on such trajectories would be smaller than that of the RFRM saddle point. Also, it is questionable whether a thermal distribution of K at the turning point of such trajectories at high J would be generated.

Although the ''empirical'' $\mathcal{J}_{\rm eff}$ values required to reproduce the high energy anisotropy data correspond to shapes more elongated than the RFRM calculated saddle points for high J, they are less elongated than the $J=0$ saddle-point shape. This implies that there is no dramatic change in the reaction mechanism, and supports the above evolutionary picture, based on an increasing fraction of trajectories failing to reach the equilibrium configuration with increasing J. It is interesting to ask whether the ''empirical'' $\mathcal{J}_{\rm eff}$ values can be related to the average most compact shape (i.e., the average turning point in the trajectories) for a given J. This question may be possible to answer by more comprehensive measurements, or more likely, through a theoretical approach. Realistic dynamical modelling of heavy-ion induced fission, including the mass asymmetry and K degrees of freedom, would surely clarify the dynamics of the fission process under these circumstances.

An alternative explanation, also of an evolutionary nature, is that the reactions at the higher energies result in nonequilibrium fission. This process was postulated [7] to explain similar data. It was suggested that there is a ''memory'' of the initial K value in the entrance channel, due to the short time spent in the equilibrium potential pocket. Dynamical calculations should be carried out to test whether such a process is possible, or whether the qualitative discussion given above of the small energy costs for generating wide K distributions at equilibrium means that K will in general be equilibrated before the fission barrier is passed.

It can be argued that the fission barrier height will be reduced by the effect of temperature, and the deduced limiting angular momentum actually corresponds to disappearance of the barrier in the hot system. Temperature dependent barrier heights must be discussed with some care [43], however, it is clear that if the level density at the saddle-point is greater than that at equilibrium, effectively the fission barrier is no longer present. If this is the case, not only should it be impossible to describe the anisotropy data with the statistical model, but clearly no aspect of the fission process should be modelled within the equilibrium statistical picture.

VI. CONCLUSIONS

Fusion cross sections, fission probabilities, and fission fragment anisotropies have been measured to high accuracy for the ^{19}F+^{208}Pb reaction, over a wide range of bombarding energies. Fitting of the fusion cross sections and the fusion barrier distribution allowed reliable prediction of the fusion angular momentum distributions. Statistical model calculations of the fission anisotropies were unable to reproduce the observed dependence on beam energy, even when the effect of a transient fission delay time was accounted for. This was

caused by the RFRM predicting a rapid transition to compact saddle-point shapes for high angular momenta, resulting in calculated anisotropies falling with beam energy above a certain value, rather than rising monotonically as observed.

The deviation from the statistical model calculations was found to occur at an angular momentum $J\hbar$ between $50\hbar$ and $60\hbar$, where the fission barrier height is less than the nuclear temperature. The data could be fitted by defining an ''empirical'' J dependence of the effective moment of inertia above this limit. Taken at face value, the ''empirical'' $\mathcal{J}_{\rm eff}$ at high J correspond to shapes controlling the K distribution which are only slightly more compact than the $\mathcal{J}_{\rm eff}$ for low J, in contrast with the RFRM calculations. This is interpreted in terms of a range of trajectories over the potential energy surface, an increasing fraction failing to reach the equilibrium configuration with increasing J. It is speculated that through a comprehensive dynamical model, it may be possible to relate the experimental results to the actual trajectories over the potential energy surface.

ACKNOWLEDGMENTS

The contributions of all the staff in the Department of Nuclear Physics, and particularly the accelerator manager, Dr. David Weisser, in successfully recommissioning the ex-Daresbury LINAC at the ANU, are gratefully acknowledged.

[1] R. Vandenbosch and J. R. Huizenga, *Nuclear Fission* (Academic, New York, 1973).
[2] D. J. Hinde, R. J. Charity, G. S. Foote, J. R. Leigh, J. O. Newton, S. Ogaza, and A. Chatterjee, Nucl. Phys. **A452**, 550 (1986).
[3] E. Mordhorst, M. Strecker, H. Frobreen, M. Gasthuber, W. Scobel, B. Gebauer, D. Hilscher, M. Lehmann, H. Rossner, and Th. Wilpert, Phys. Rev. C **43**, 716 (1991).
[4] D. J. Hinde, D. Hilscher, H. Rossner, B. Gebauer, M. Lehmann, and M. Wilpert, Phys. Rev. C **45**, 1229 (1992).
[5] J. P. Lestone, J. R. Leigh, J. O. Newton, D. J. Hinde, J. X. Wei, J. X. Chen, S. Elfström, and M. Zielinska-Pfabe, Nucl. Phys. **A559**, 277 (1993).
[6] H. Halpern and V. M. Strutinski, *Proceedings of the Second United Nations International Conference on the Peaceful Uses of Atomic Energy*, Geneva, Switzerland, 1955 (United Nations, Geneva, Switzerland, 1958), p. 408.
[7] V. S. Ramamurthy and S. S. Kapoor, Phys. Rev. Lett. **54**, 178 (1985).
[8] R. Bock, Y. T. Chu, M. Dakowski, A. Gobbi, E. Grosse, A. Olmi, H. Sann, D. Schwalm, U. Lynen, W. Müller, S. Bjornholm, H. Esbensen, W. Wölfli, and E. Morenzoni, Nucl. Phys. **A388**, 334 (1982).
[9] B. B. Back, R. R. Betts, J. E. Gindler, B. D. Wilkins, S. Saini, M. B. Tsang, C. K. Gelbke, W. G. Lynch, M. A. McMahan, and P. A. Baisden, Phys. Rev. C **32**, 195 (1985).
[10] J. Tōke, R. Bock, G. X. Dai, A. Gobbi, S. Gralla, K. D. Hildenbrand, J. Kuzminski, W. J. F. Müller, A. Olmi, and H. Stelzer, Nucl. Phys. **A440**, 327 (1985).
[11] H. A. Weidenmüller and Zhang Jing-Shang, Phys. Rev. C **29**, 879 (1984).
[12] H. Rossner, D. Hilscher, E. Holub, G. Ingold, U. Jahnke, H. Orf, J. R. Huizenga, J. R. Birkelund, W. U. Schröder, and W. W. Wilcke, Phys. Rev. C **27**, 2666 (1983).
[13] A. Gavron, P. Eskola, A. J. Sierk, J. Boissevain, H. C. Britt, K. Eskola, M. M. Fowler, H. Olm, J. B. Wilhelmy, S. Wald, and R. L. Ferguson, Phys. Rev. Lett. **52**, 589 (1984).
[14] H. Zhang, Z. Liu, J. Xu, K. Xu, J. Lu, and M. Ruan, Nucl. Phys. **A512**, 531 (1990).
[15] C. R. Morton, D. J. Hinde, J. R. Leigh, J. P. Lestone, M. Dasgupta, J. C. Mein, J. O. Newton, and H. Timmers, Phys. Rev. C **52**, 243 (1995).
[16] V. E. Viola, K. Kwiatkowski, and M. Walker, Phys. Rev. C **31**, 1550 (1985).
[17] N. Rowley, G. R. Satchler, and P. H. Stelson, Phys. Lett. B **254**, 25 (1991).
[18] J. X. Wei, J. R. Leigh, D. J. Hinde, J. O. Newton, R. C. Lemmon, S. Elfström, and J. X. Chen, Phys. Rev. Lett. **67**, 3368 (1991).
[19] N. Rowley, J. R. Leigh, J. X. Wei, and R. Lindsay, Phys. Lett. B **314**, 179 (1993).
[20] A. B. Balantekin, A. J. DeWeerd, and S. Kuyucak, Phys. Rev. C **54**, 1853 (1996).
[21] R. Vandenbosch, Annu. Rev. Nucl. Part. Sci. **42**, 447 (1992).
[22] M. Dasgupta, A. Navin, Y. K. Agarwal, C. V. K. Baba, H. C. Jain, M. L. Jhingan, and A. Roy, Nucl. Phys. **A539**, 351 (1992).
[23] M. Dasgupta, ANU Department of Nuclear Physics Internal Report No. ANU-P/1333, 1997 (unpublished).
[24] C. H. Dasso and S. Landowne, Comput. Phys. Commun. **46**, 187 (1987); J. O. Fernández-Niello, C. H. Dasso, and S. Landowne, *ibid.* **54**, 409 (1989).
[25] M. Dasgupta, K. Hagino, C. R. Morton, D. J. Hinde, J. R. Leigh, N. Takigawa, H. Timmers, and J. O. Newton, J. Phys. G **23**, 1491 (1997).
[26] A. J. Sierk, Phys. Rev. C **33**, 2039 (1986).
[27] D. Ward, R. J. Charity, D. J. Hinde, J. R. Leigh, and J. O. Newton, Nucl. Phys. **A424**, 189 (1983).
[28] J. Tōke and W. J. Swiatecki, Nucl. Phys. **A372**, 141 (1981).
[29] J. O. Newton, D. J. Hinde, R. J. Charity, J. R. Leigh, J. J. M. Bokhorst, A. Chatterjee, G. S. Foote, and S. Ogaza, Nucl. Phys. **A483**, 126 (1988).
[30] H. Rossner, D. J. Hinde, J. R. Leigh, J. P. Lestone, J. O. Newton, J. X. Wei, and S. Elfstrom, Phys. Rev. C **45**, 719 (1992).
[31] D. J. Hinde (unpublished).
[32] H. Rossner and P. Fröbrich, Z. Phys. A **349**, 99 (1994).
[33] B. B. Back, Phys. Rev. C **31**, 2104 (1985).
[34] M. Prakash, V. S. Ramamurthy, S. S. Kapoor, and J. M. Alexander, Phys. Rev. Lett. **52**, 990 (1984).
[35] K. H. Bhatt, P. Grange, and B. Hiller, Phys. Rev. C **33**, 954 (1986), and references therein.
[36] A. Gavron, J. R. Beene, B. Cheynis, R. L. Ferguson, F. E. Obenshain, F. Plasil, G. R. Young, G. A. Petitt, R. Jääskel-

aäinen, D. G. Sarantites, and C. F. Maguire, Phys. Rev. Lett. **47**, 1255 (1981); **48**, 835(E) (1982).
[37] E. Holub, D. Hilscher, G. Ingold, U. Jahnke, H. Orf, and H. Rossner, Phys. Rev. C **28**, 252 (1983).
[38] W. P. Zank, D. Hilscher, G. Ingold, U. Jahnke, M. Lehmann, and H. Rossner, Phys. Rev. C **33**, 519 (1986).
[39] A. Gavron, A. Gayer, J. Boissevain, H. C. Britt, T. C. Awes, J. R. Beene, B. Cheynis, D. Drain, R. L. Ferguson, F. E. Obenshain, F. Plasil, G. R. Young, G. A. Petitt, and C. Butler, Phys. Rev. C **35**, 579 (1987).
[40] D. J. Hinde, J. R. Leigh, J. J. M. Bokhorst, J. O. Newton, R. L. Walsh, and J. E. Boldeman, Nucl. Phys. **A483**, 126 (1987).
[41] D. J. Hinde, H. Ogata, M. Tanaka, T. Shimoda, N. Takahashi, A. Shinohara, S. Wakamatsu, K. Katori, and H. Okamura, Phys. Rev. C **37**, 2923 (1989).
[42] D. Hilscher, H. Rossner, B. Cramer, B. Gebauer, U. Jahnke, M. Lehmann, E. Schwinn, M. Wilpert, Th. Wilpert, H. Frobreen, E. Mordhorst, and W. Scobel, Phys. Rev. Lett. **62**, 1099 (1989).
[43] R. J. Charity, Phys. Rev. C **53**, 512 (1996).